JOURNAL OF GEOPHYSICAL RESEARCH: SPACE PHYSICS, VOL. 118, 5522–5531, doi:10.1002/jgra.50528, 2013

Exploring the influence of ionospheric O^+ outflow on magnetospheric dynamics: The effect of outflow intensity

Yiqun Yu[1] and Aaron J. Ridley[2]

Received 25 June 2013; revised 2 August 2013; accepted 22 August 2013; published 6 September 2013.

[1] The ionospheric O^+ outflow varies dramatically during geomagnetic activities, but the influence of its initial characteristics on the magnetospheric dynamics has not been well established. To expand a previous study on the impact of ionospheric heavy ions outflow originating from different source regions on the magnetotail dynamics and dayside reconnection rate, this study conducts two idealized numerical experiments with different O^+ outflow densities to examine the consequent change in the magnetosphere system, especially on the solar wind-magnetosphere coupling efficiency. Results indicate that a larger O^+ outflow is capable of triggering the Kelvin-Helmholtz instability (KHI) on the magnetopause flanks. The subsequent surface waves enhance the solar wind-magnetosphere coupling efficiency by transmitting more solar wind energy into the magnetosphere-ionosphere system, increasing the cross polar cap potential index. This index is initially reduced after the ionospheric mass loading owing to the direct depression in the dayside reconnection rate as commonly reported from earlier literature. The above KHI is generated under steady state solar wind conditions, suggesting that besides the commonly recognized cause, the elevated solar wind speed, ionospheric heavy ions outflow is another potential factor in disturbing the boundary by enhancing the mass density near the magnetopause and thus lowering the threshold for generating KHI. During storms, the increased ionospheric mass source causes an increased probability of KHI, which allows more solar wind plasma into the magnetosphere. This implies there is a possibility of even further nonlinear coupling between the magnetosphere and solar wind.

Citation: Yu, Y., and A. J. Ridley (2013), Exploring the influence of ionospheric O^+ outflow on magnetospheric dynamics: The effect of outflow intensity, *J. Geophys. Res. Space Physics*, *118*, 5522–5531, doi:10.1002/jgra.50528.

1. Introduction

[2] Ions (H^+, He^+, O^+) flowing out of Earth's ionosphere provide another mass source to the magnetosphere in addition to the solar wind particles, altering the magnetospheric dynamics particularly during magnetically active times [e.g., *Daglis and Axford*, 1996; *Moore et al.*, 2005; *Li et al.*, 2011]. Recently, the role of heavy ions (i.e., O^+) in the magnetosphere has been increasingly explored using either simulations [e.g., *Glocer et al.*, 2009a; *Winglee et al.*, 2002; *Yu and Ridley*, 2013; *Brambles et al.*, 2010; *Wiltberger et al.*, 2010] or observations [e.g., *Kistler et al.*, 2005, 2010; *Liao et al.*, 2010, 2012]. For example, *Yu and Ridley* [2013] examined the influence of heavy ion outflow originating from different ionospheric source locations on the magnetospheric dynamics using global magnetohydrodynamic (MHD) simulations. They found that heavy ions flowing out of the dayside cusp region have a much more significant impact on the magnetotail dynamics as well as on the dayside reconnection rate than that flowing out of the nightside auroral region.

[3] While the heavy ion outflow is growingly recognized as an important source in changing the magnetospheric dynamics, such as the ring current [*Winglee*, 2003; *Nosé et al.*, 2005] and the reconnection rate [*Borovsky et al.*, 2008; *Yu and Ridley*, 2013; *Liu et al.*, 2013], its initial characteristics (i.e, the velocity, temperature, density of the ions when leaving the ionosphere), which can vary dramatically depending on the energy deposit into the ionosphere, are likely to play a controlling role in influencing the system dynamics. Initial characteristics specified in global simulations resemble the outflow condition near altitude of 2.5–3.5 R_e, the inner boundary of most global models. The outflow conditions at the starting point (i.e., the inner boundary in global models) are found to influence the global magnetospheric state. For example, *Garcia et al.* [2010] carried out several global MHD simulations with different

[1]Space Science and Application, Los Alamos National Laboratory, Los Alamos, New Mexico, USA.
[2]Center for Space Environment Modeling, University of Michigan, Ann Arbor, Michigan, USA.

Corresponding author: Y. Yu, Space Science and Application, Los Alamos National Laboratory, Los Alamos, NM 87545, USA. (yiqun@lanl.gov)

2169-9380/13/10.1002/jgra.50528

levels of O^+ outflow flux from the nightside auroral region and demonstrated that the increase of ionospheric O^+ flux decreases the ionosphere cross polar cap potential (CPCP), which is consistent with other studies [e.g., *Winglee et al.*, 2002; *Glocer et al.*, 2009a; *Brambles et al.*, 2010; *Welling and Zaharia*, 2012]. The fluence in their studies, which represents the amount of ions out of the ionosphere, is similar to observed statistics, that is, around the order of 10^{25} ions/s [*Cully et al.*, 2003]. *Wiltberger et al.* [2010] conducted MHD simulations to examine the influence of different cusp outflow flux on the state of the magnetosphere and found that with a larger outflow flux, the magnetospheric configuration can be dramatically disturbed by developing more substorm events as opposed to that with no or smaller outflow flux. *Brambles et al.* [2010] found that the responses in the magnetosphere-ionosphere system is associated with the outflow velocity and temperature of the ionosphere origin O^+. *Brambles et al.* [2011] investigated the dependence of sawtooth occurrence on the ionospheric outflow fluence and concluded that the magnetosphere undergoes sawtooth oscillation when the ionospheric outflow fluence exceeds a threshold, otherwise is quasi-steady. The above studies made an important step in examining the dependence of the magnetosphere state on the ionospheric outflow characteristics, by using the Lyon-Fedder-Mobarry model [*Lyon et al.*, 2004]. This study continues the exploration of the impact of the ionospheric heavy ion outflow on magnetospheric dynamics by using a different global MHD model Block-Adaptive Tree Solar-wind Roe Upwind Scheme (BATS-R-US) (details of this model are provided in the next section).

[4] Previous studies showed the correlation between heavy ions originating from the ionosphere and surface waves on the magnetopause boundary [e.g., *Bouhram et al.*, 2005]. The surface waves are mainly caused by Kelvin-Helmholtz instability that usually occurs with the presence of large relative shear velocities and is often observed on the flank magnetopause where the solar wind speed on the magnetosheath side is sufficiently different than the convection inside the magnetosphere. The Kelvin-Helmholtz instability (KHI) is an important magnetospheric physical process because it allows for the transport of solar wind mass and energy into the magnetosphere by mixing the plasma from two different regions via the roll-up vortices [*Pegoraro et al.*, 2008; *Hasegawa et al.*, 2004; *Nykyri and Otto*, 2001; *Nakamura et al.*, 2008]. This interaction is therefore considered as the second most important solar wind-magnetosphere coupling process other than magnetic reconnection. The instability preferentially occurs with the interplanetary magnetic field (IMF) orientation being northward [*Kivelson and Chen*, 1995; *Hasegawa et al.*, 2004]. However, the first in situ observations of KHI during southward IMF was reported by *Hwang et al.* [2011] from Cluster data with a dynamically active subsolar environment. In their study, the AE index is observed to be high during time periods when KH surface waves are observed, suggesting strong substorm activities. While substorms are highly correlated with ionospheric heavy ions outflow [*Kistler et al.*, 2010], the authors suggested that the increased mass density in the plasma sheet and near the magnetopause may facilitate the KHI. Bearing in mind of the above correlation, this study will explore the instability by varying the ionospheric O^+ outflow density, aiming to investigate the impact on the solar wind-magnetosphere coupling as well as in the ionospheric electrodynamics.

2. Methodology

[5] The global multifluid MHD model Block-Adaptive Tree Solar-wind Roe Upwind Scheme (BATS-R-US) [*Powell et al*., 1999] is employed. The multifluid code solves MHD equations for two ion fluids (i.e., H^+ and O^+) with their individual mass, momentum, and energy equations [*Glocer et al.*, 2009b]. This MHD model is coupled with an ionospheric electrodynamic solver [*Ridley et al.*, 2004]: the field-aligned currents computed just outside (3.5 R_e) the inner boundary of the MHD code are mapped down to the ionospheric height where the ionospheric electric potential is computed; the potential is then mapped out to the inner boundary of the MHD code to obtain the $E \times B$ convection velocity, which is used as the inner boundary condition for the perpendicular velocity of the ions. The conductivity used in the ionospheric solver is not uniform but structured, depending on the mapped field-aligned currents. The conductance includes solar-generated conductance, nightside conductance, and auroral zone conductance (details about the influence of the ionospheric conductance on the magnetosphere can be found in *Ridley et al.* [2004]). The MHD code is also coupled with the Rice Convection Model (RCM) [*Wolf*, 1983; *Toffoletto et al.*, 2003], which captures the kinetic behavior of charged particles in the inner magnetosphere by solving the distribution functions of a number of "fluids" in a self-consistently computed electric field, given magnetic fields generated from the BATS-R-US MHD model. The pressure and density of each fluid (H^+ and O^+) in the inner magnetosphere solved in BATS-R-US are corrected by the kinetic RCM because charged particles no longer behave like ideal MHD fluids in that region. Instead, the charged particles transport separately around the Earth according to their mass and sign of charges under the combined effect of the embed high magnetic fields, corotation electric fields, and externally driven electric fields in the inner magnetosphere. The coupling between the RCM and the global magnetosphere MHD model BATS-R-US is described in more detail by *De Zeeuw et al.* [2004]. The above coupled near-Earth framework is highly capable of capturing the terrestrial magnetospheric dynamics, such as the magnetospheric plasma and fields [*Welling and Ridley*, 2010], and the induced magnetic field variation on the Earth surface [*Yu and Ridley*, 2008; *Yu et al.*, 2010].

[6] The physical domain covered by the MHD model extends from 32 R_e on the dayside to 224 R_e on the nightside in the Sun-Earth direction and ± 128 R_e in the other two directions. The state of the magnetosphere is controlled by solar wind conditions at the upstream outer boundary (32 R_e) and ionosphere conditions at the inner boundary (spherically 2.5 R_e). The solar wind conditions at the upstream boundary can be obtained either from other model output [e.g., *Ridley*, 2006] or from real observations such as Advanced Composition Explorer (ACE) or Wind measurements [e.g., *Yu and Ridley*, 2008] or even from user-designed conditions [e.g., *Yu and Ridley*, 2011]. Other outer boundaries use zero gradient in the solar wind plasma parameters because these boundaries are too far from the Earth to influence the

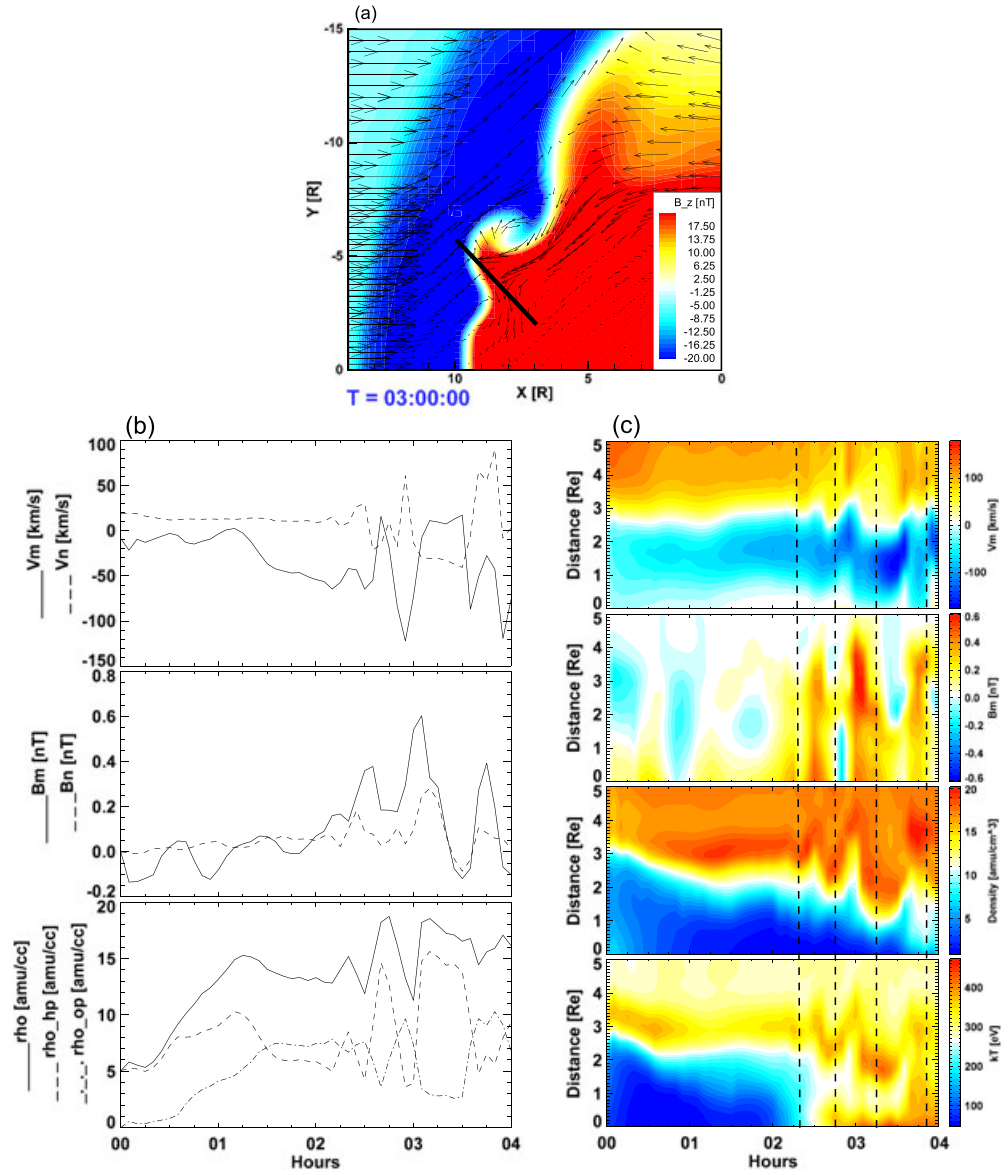

Figure 1. (a) The Z component magnetic field in the equatorial plane for the dusk side at time 03:00. (b) The velocity and magnetic field vectors in their M and N directions with respect to the magnetopause on the middle point of the black line in Figure 1a. The bottom plot shows H^+, O^+ and total mass densities at the same location. (c) Contour plots of shear velocity, magnetic field, total mass density, and energy density along the black line across the magnetopause as a function of time. The upper part in these plots represents the magnetosheath region and the lower part is within the magnetosphere region. Four vortices are developed around 02:20, 02:45:, 03:15, and 03:50 (marked by vertical lines) as identified from the plot of mass density. These vortices help the magnetospheric side mass to intrude into the magnetosheath region.

near-Earth dynamics. The inner boundary of the MHD code, a spherical shell at 2.5 R_e, requires the specification of density, velocity, and temperature for both ion fluids. These parameters on the inner boundary of the MHD model are essentially the controlling factors in this study, as they describe the outflow conditions.

[7] In this study, the upstream solar wind and IMF conditions remain constant in driving the magnetosphere: B_x = B_y = 0, B_z = –5 nT, N_{H^+} = 5 cm^{-3}, N_{O^+} = 0.0001 cm^{-3}, V_{xH^+,O^+} = 400 km/s, and T_{H^+,O^+} = 100,000 K. At the inner boundary, a uniform ionospheric outflow is specified over both the Southern and Northern polar caps (above 60° magnetic latitude at 2.5 R_e, which corresponds to magnetic latitude above 71.6° at the ionospheric height). The parameters for the outflow ions are specified as follows: $V_{O^+\|}$ = 20 km/s, T_{O^+} = 1,000,000 K, $V_{H^+\|}$ = 2 km/s, T_{H^+} = 100,000 K, and N_{H^+} = 20 cm^{-3}. Two simulations are performed with different O^+ densities: one simulates an ionospheric outflow event with N_{O^+} = 20 cm^{-3}, and the other one has N_{O^+} = 40 cm^{-3}. The above inner boundary conditions in the two simulations correspond to a O^+ fluence of 9.87×10^{25} and 1.93×10^{26} ions/s, respectively, which fall in the range of

the observation statistics [*Cully et al.*, 2003]. Both outflows are initialized at the beginning of time-dependent simulation after the system converges to a steady state using thousands of iterative steps (in non-time-dependent mode). It should be noted that such a specification of uniform and large outflow source in the polar cap region is only for experimental studying of the impact of outflow intensity, because observations rarely see the presence of a large outflow flux simply over the polar cap. Nevertheless, since the modeled amount of fluence agrees with observational statistics, the current study still mimics reality in the global outflow rate, allowing us to learn, in a general sense, about the impact of the ionospheric mass loading rate, regardless of its source region and pathway, on the magnetosphere system.

3. Simulation Results

[8] While the magnetosphere is relatively steady after the ionospheric outflow with density of 20 cm^{-3} populates the magnetosphere, the magnetosphere with 40 cm^{-3} ionospheric outflow density undergoes substantial turbulence on its low-latitude boundary layer. Figure 1a shows a color contour of magnetic field Z component in the dawnside equatorial plane at 03:00. The dayside magnetopause is highly disturbed as a vortex propagates along the magnetopause toward the tail, mixing two plasma sources from the magnetosheath and magnetosphere. Figure 1b illustrates the evolution of the velocity, magnetic field, and density at the middle point of the black line in Figure 1a that crosses the magnetopause boundary, resembling measurements from a stationary satellite. The velocity and magnetic field are in a local LMN (boundary normal) coordinate system [*Russell and Elphic*, 1979], where **M** points toward dawn along the equatorial magnetopause surface, **N** points in the normal direction of the magnetopause in the equatorial plane, and **L** completes the third axis in orthogonal system (i.e., the **Z** direction out of the equatorial plane toward the north). The plasma velocity is mainly in the **M** direction, i.e., along the magnetopause; the magnetic field in both **M** and **N** directions are small since the dominant component is in the **Z** direction; the total mass density, including both H^+ and O^+, is significantly enhanced by a factor of 3 (from 5 to 15 cm^{-3} around 01:15) after the O^+ ions flow toward the magnetopause from the nightside (i.e, starting from 00:35 to 01:30). Around 02:00, the virtual stationary satellite observes quasiperiodic variations in all of these parameters, implying that the magnetopause is oscillating around the virtual stationary satellite.

[9] Figure 1c shows 2-D contour plots of plasma shear velocity, magnetic field in the **M** direction, density, and energy along the black line as a function of time. The magnetosheath is in the upper part of each plot, while the magnetosphere is in the lower part. During the simulation, the magnetosheath plasma with smaller magnetic field, higher density, and hotter particles intrudes into the magnetosphere at least four times at this selected magnetopause location with an approximate period of 30 min (i.e., the intrusion takes place around 02:20, 02:45, 03:15, 03:50, identified from the density contour plot and marked by vertical dashed line). The penetration of plasma into the magnetosphere is as deep as $1.5R_e$, and the magnetospheric plasma also migrates toward the magnetosheath as the vortex rotates while traveling along the magnetopause, mixing the plasma from the two domains.

[10] These four penetrations of magnetosheath mass and energy into the magnetosphere are due to four successive transient vortices traveling along the magnetopause, which stems from the Kelvin-Helmholtz instability (KHI).

4. Discussion

[11] Theoretically, the KHI grows when the shear flow is larger than a certain threshold according to a linear inequality [*Hasegawa*, 1975; *Gratton et al.*, 2004]:

$$(\mathbf{V}\cdot\mathbf{k})^2 \geq \frac{\rho_1+\rho_2}{\mu\rho_1\rho_2}[(\mathbf{B_1}\cdot\mathbf{k})^2+(\mathbf{B_2}\cdot\mathbf{k})^2] \tag{1}$$

where **k** is the wave vector. **V**, **B**, and ρ denote the velocity difference between the two plasma, magnetic field, and total mass density. The indices "1" and "2" represent the magnetosphere and magnetosheath domains, respectively. The velocity and magnetic field vectors contain the directions along the magnetopause toward dawnside (**M** direction), **Z** (**L**) direction, and the normal of the magnetopause (**N** direction). Assuming that the field component in the **N** direction is negligible, that the wave propagation is confined within the LM plane and that the angle between the wave propagation **k** and **M** direction is θ, the above inequality becomes

$$[(V_{m1}-V_{m2})\cos\theta+(V_{z1}-V_{z2})\sin\theta]^2 \geq \frac{\rho_1+\rho_2}{\mu\rho_1\rho_2}\left[(B_{m1}\cos\theta+B_{z1}\sin\theta)^2+(B_{m2}\cos\theta+B_{z2}\sin\theta)^2\right]. \tag{2}$$

If the wave propagates vertically (i.e., in **Z** direction, $\theta = 90°$), it is suppressed quickly by the Z component of the magnetospheric field, which is very large and provides an effective surface tension that can stabilize the wave along the same direction. If the wave propagates along the equatorial magnetopause (θ is zero), then the above inequality becomes

$$(V_1-V_2)^2 \geq \frac{B_1^2+B_2^2}{\mu\rho_2}\left(1+\frac{\rho_2}{\rho_1}\right) \tag{3}$$

where V and B are both in the **M** direction. In this case, the Z component of magnetic field has no effect on the wave propagation.

[12] With inequality (2), the theoretical prediction of the KHI onset near the dawn magnetopause is tested using the simulation results. The parameters for the magnetosphere and magnetosheath regions used in inequality (2) are taken from two points on the black line (shown in Figure 1a) 0.75 R_e away from the magnetopause, identified from the magnetic field reversal in the **Z** direction). The threshold (right-hand side, RHS, of inequality (2)) is computed with the density ρ either including O^+ or excluding O^+ (this can be easily achieved because the multifluid simulation treats each ion species individually) and is then compared to the square of shear velocity (left-hand side, LHS, of inequality (2)). Figure 2 illustrates the contour of LHS minus RHS in inequality (2) as a function of wave propagation angle and time. The positive value represents the square of the linear growth rate of the KH waves [*Claudepierre et al.*, 2008]. The RHS/threshold in Figure 2a includes O^+ in the density parameter, while the RHS/threshold in Figure 2b

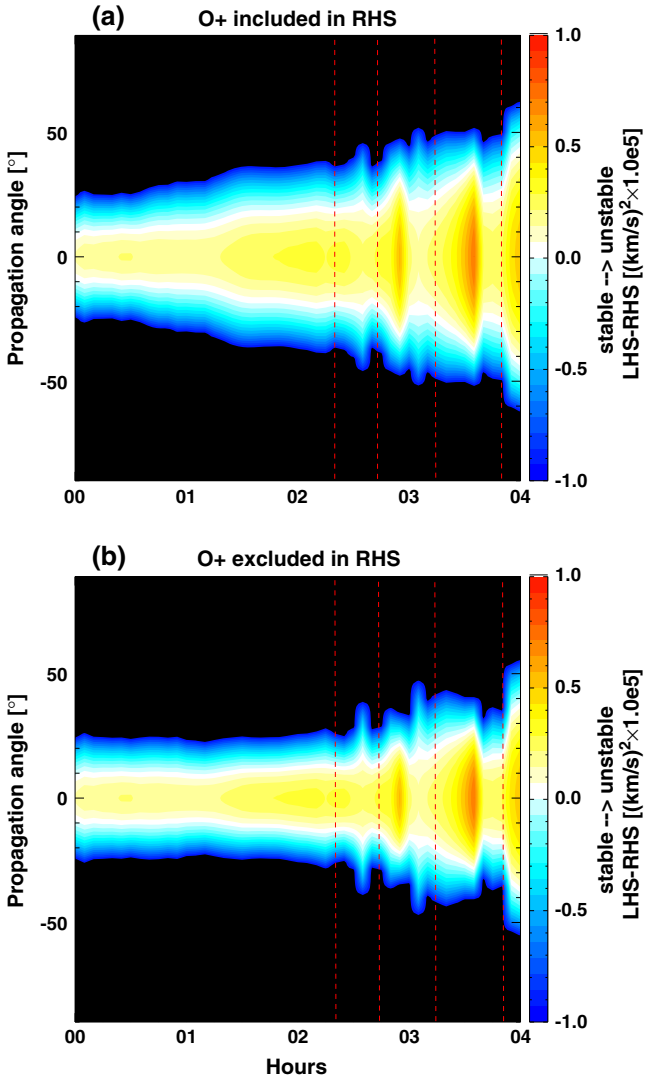

Figure 2. Contour of the difference between the LHS and RHS ((a) with O^+ included; (b) with O^+ excluded) of inequality (2) with angles ranging from –90° to 90°. The parameters needed in the inequality are taken from both sides 0.75 R_e away from the magnetopause on the black line shown in Figure 1. Yellow indicates the magnetosphere is unstable while blue means the system is stable. The four vertical lines indicate the intrusion of magnetosheath plasma into the magnetosphere.

excludes O^+. In either case, when the wave propagates with a larger angle θ with respect to the equatorial plane, the magnetosphere is more stable (blue/black) because the larger magnetic field Z component along the wave propagation plays an increasingly effective role of stabilizing the surface waves. With an angle closer to the equatorial plane, the Kelvin-Helmholtz instability will grow more easily (red) since the Z component of magnetic field in the equatorial plane is less capable of stabilizing the waves. Each intrusion time of magnetosheath plasma into the magnetosphere as marked by the vertical lines roughly indicates the growth of an unstable state across the equator (i.e., transiting to yellow/red along the time). In addition, with O^+ included, the off-equator Kelvin-Helmholtz instability appears stronger.

[13] Figure 3 shows the shear velocity (square root of the LHS of inequality (2), symboled by "△"), the square root of the threshold/RHS with O^+ (symboled by "⋆"), and without O^+ (symboled by "◇") included in the parameter ρ. When the △ is above the ⋆ and ◇, the system is KH unstable, independent of whether O^+ is considered or not. Figures 3a and 3b illustrate these quantities with the wave angle being 0° and 20°, respectively. The magnetosphere is predicted to be unstable throughout the entire simulation when the waves travel along the magnetopause boundary (θ = 0°) because

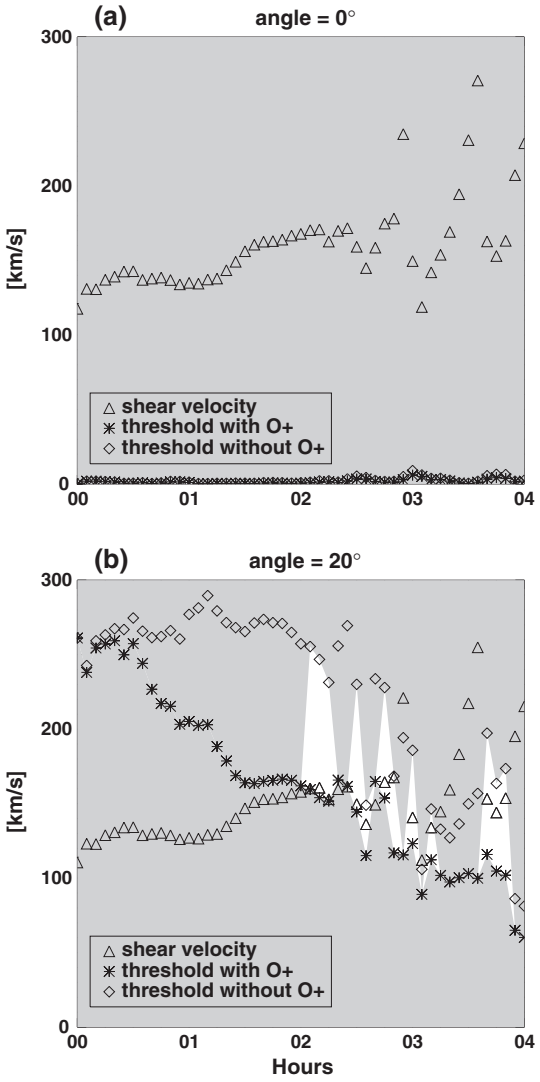

Figure 3. The shear velocity (square root of LHS, symboled by triangle) and two thresholds (square root of RHS) when O^+ is included in the mass density (star) and when no O^+ is included (diamond). (a) The inequality with a wave angle of 0° and (b) an angle of 20°. The unshaded region represents time periods when the instability is triggered only with the help of heavy ions. (The shear velocity is larger than the threshold with O^+ but is smaller than the threshold without O^+. That is, no KHI will occur if O^+ is not included in the threshold.) The shaded region represents all other circumstances, including stable state due to a smaller shear velocity compared to both thresholds, unstable state when the shear velocity is larger than both thresholds.

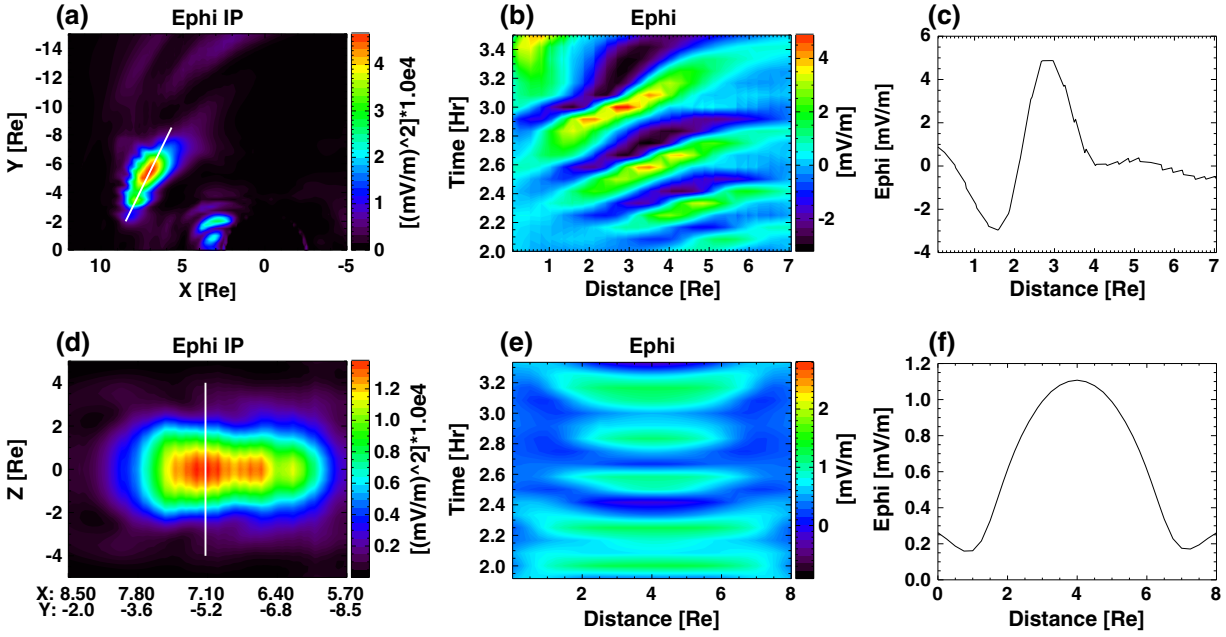

Figure 4. (a) The integrated power spectral of the azimuthal electric field on the morning magnetosphere in the equatorial plane. The black line crosses the main region of the wave pulsation on the morning magnetopause boundary. (b) The azimuthal electric field $E\phi$ on the black line as a function of time. The slope of wave traces can be used to calculate the wave phase speed, which is approximately 16 km/s. (c) $E\phi$ at time 03:00 on the black line. The oscillation in this plot is used to determine the wavelength propagating along the magnetopause in the equatorial plane, which is 2.6 R_e. (d, e, f) The azimuthal electric field on the vertical (Z) plane with the intersection line with the equator on the black line in Figure 4a. These plots indicate that the wavelength of the wave component propagating in the Z direction, which is 6.5 R_e. The two wavelengths along the Z direction and the equatorial magnetopause direction indicate a propagation angle of 22° with respect to the equatorial plane.

the shear velocity is always above the threshold either with or without O^+. On the other hand, when the △ is located below the ⋆ or ◇, the system is stable, as is the case in Figure 3b, i.e., 20° propagation angle, at the start of the simulation. Eventually, the △ goes between the ⋆ and ◇, implying that the system is KH unstable if O^+ is considered, but would be stable if there were no O^+. This is the case after about 2 h. It is consistent with the disturbance onset time shown by the simulation (see Figure 1). Initially, when only a few O^+ ions arrive at the magnetopause, the thresholds with O^+ and without O^+ are almost the same, and the shear velocity is well below the threshold, implying a stable magnetosphere. When O^+ ions start to appear near the magnetopause, the threshold with O^+ included in the density parameter is significantly decreased (see ⋆ line), while the threshold excluding O^+ ions is much greater, leaving the shear velocity (△) in the middle of the two during most time of the simulation after 02:00. In other words, the shear velocity (△) is larger than the threshold with O^+ ion (⋆) and smaller than that without O^+ (◇) (denoted by the unshaded region), indicating that the presence of O^+ increases the possibility of the KHI onset near the flank/magnetopause by lowering the threshold of the instability. This is consistent with an observational study by *Bouhram et al.* [2005] who showed that with a sufficiently large amount of heavy ions in the magnetosphere, the KHI is more likely to occur.

[14] The above theoretical prediction of the onset of KHI indicates that the KHI can take place from the beginning if the wave travels in the equatorial plane along the magnetopause but can not be excited until around 02:00 if the wave propagates with an angle of at least 20° off the equator. The latter is more consistent with the simulation results that show no disturbances on the magnetopause until about 2 h after the outflow. To explain the discrepancy between the simulation results (KHI begins at around 02:00) and the theoretical prediction (KHI begins at 00:00 with 0° propagation angle but later with a larger propagation angle), there could be several possibilities. First, it might be associated with the way the parameters on both sides of the magnetopause are chosen in examining the stability of the boundary. In other words, taking parameters 0.75 R_e away from the magnetopause probably introduces some uncertainties, as the magnetopause boundary may frequently change in thickness due to the passage of vortex. The second possible reason for the discrepancy is that the viscosity (mainly the numerical resistivity) on the boundary inhibits or delays the onset of the KH instability in the simulation, while the theoretical criteria shown by inequality (1) is derived from incompressible plasma and does not take into account other factors in the fluids except for the magnetic field and mass density. The last possibility is that the KH surface waves in the simulation indeed propagate with an angle of 20° off the equator.

[15] As a comparison to the simulation that develops KH waves, the theoretical prediction of the stability is also investigated in the simulation that has less O^+ outflow from the

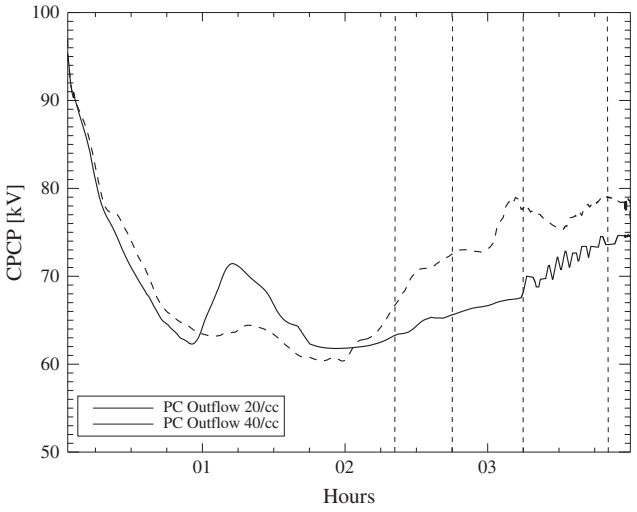

Figure 5. The cross polar cap potential index for two simulations with outflow density of 20 (solid) and 40 cm^{-3} (dashed), respectively. The vertical lines represent the four intrusions identified in Figure 1 for the case with 40 cm^{-3}.

ionosphere. No vortex is found on the magnetopause boundary, and the magnetosphere is mostly quiet. The same line is extracted on the morning magnetopause and parameters are chosen 0.75 R_e away from the magnetopause to be used as the input in inequality (2). This theoretical results indicate potential growing of KHI from the beginning of the simulation with a propagation angle within 0°–15°. This implies that the first explanation mentioned above is invalid as the boundary thickness in this second simulation nearly remains constant due to the absence of disturbance. While it is a difficult task to quantitatively determine the role of numerical resistivity in suppressing the waves, it is possible to analyze the wave propagation on the magnetopause surface in the 3-D model, in order to determine whether the KHI was initiated because of the difference in possible propagation angles.

4.1. Wave Propagation

[16] To determine the wave propagation angle on the magnetopause surface from our simulation results, the wave numbers on the **M** direction (along the equatorial magnetopause boundary) and on the **L** direction (Z direction) should be identified.

[17] To determine the wave number along the **M** direction, two steps are followed. Firstly, the power spectral analysis technique developed in *Claudepierre et al.* [2008] is applied to the azimuthal electric field on the equatorial magnetosphere to find out the location of the wave pulsation. After integrating the power spectral density of the azimuthal electric field $E\phi$ over the Pc4–5 frequency range (0.15–15mHz), the low-frequency KH wave pulsation is found to be located on both morning and afternoon flanks. Figure 4a illustrates the total power of the azimuthal electric field in the morning equatorial magnetosphere. The wave pulsation clearly occurs on the prenoon magnetopause boundary. Secondly, the wave properties are examined along the magnetopause boundary on the equator, including the wave frequency, phase velocity, and wave number. Figure 4b shows $E\phi$ along the black line in Figure 4a as a function of time. Four coherent wave structures propagate tailward along the magnetopause boundary after 02:00, with a period approximately of 0.5 h. From the slope of these wave traces, the phase velocity of KH waves is estimated to be 16 km/s. The onset location for each wave trace appears to move closer to the dayside magnetopause with time (the X axis starts from the dayside end of the black line). Figure 4c displays $E\phi$ at time 03:00 along the black line, from which, the wavelength in the **M** direction λ_m is estimated to be $2.6R_e$. Therefore, the KH waves propagate in the equatorial plane along the magnetopause with a wave number of $k_m = 2\pi/\lambda_m = 2.4\ R_e^{-1}$.

[18] To determine the wave number along the Z direction, the same technique is employed in the vertical plane (**Z** direction) tangential to the magnetopause with the intersection line being the white line on the equator in Figure 4a. The integrated power spectral density of $E\phi$ in Figure 4d shows that the waves extend into the Z direction, implying the off-equator propagation. The wave traces (Figure 4e) obtained from the white vertical line in Figure 4d are not useful in determining the phase velocity in the Z direction because the slope is too small. Although the waves quickly dissipate after traveling in the Z direction for maximum propagation of about 3 R_e and it is difficult to identify multiple wave oscillations along the black line. Figure 4f shows a quasi-oscillation in the $E\phi$ along the black line at 03:00. Based on this the wavelength in the Z direction, λ_z is estimated to be 6.5 R_e. This corresponds to a wave number in the Z direction $k_z = 2\pi/\lambda_z = 0.967\ R_e^{-1}$.

[19] Therefore, the wave propagation angle with respect to the equator is $\tan^{-1}(k_z/k_m) \simeq 22°$. This estimation of the wave propagation angle from the 3-D simulation results is consistent with the theoretical prediction of the onset of KHI. That is, with a propagation angle about 20°, the KHI is predicted to be excited around 02:00 with the participation of O^+.

4.2. Feedback to the Ionosphere

[20] The KH surface waves on the magnetopause, triggered by a large mass loading from the ionosphere, feed back onto the ionospheric electrodynamics. Although the dayside reconnection rate can be suppressed by the increased amount of heavy ions in the magnetosphere [*Yu and Ridley*, 2013], the Kelvin-Helmholtz instability allows more solar wind mass and energy to enter the magnetosphere and increases the reconnection rate via the rolled up vortices [*Pegoraro et al.*, 2008; *Hasegawa et al.*, 2004] (as shown in Figure 1a). *Nykyri and Otto* [2001] and *Nakamura et al.* [2008] conducted MHD simulations of KH vortices and found that the reconnection also occurs above and below the equatorial plane due to the rolled up vortex. The consequence of the changed reconnection rate can be observed in the cross polar cap potential (CPCP) index in Figure 5. The CPCP index is significantly reduced after the outflow is initiated, which has been observed in previous studies [e.g., *Winglee et al.*, 2002; *Glocer et al.*, 2009a; *Brambles et al.*, 2010; *Welling and Zaharia*, 2012]. Two hours later, the CPCP index in the simulation with 20 cm^{-3} outflow density increases slightly, while the CPCP index in the other simulation, in which the KH waves are excited, increases significantly, indicating that more energy is transmitted down to the ionosphere. This is

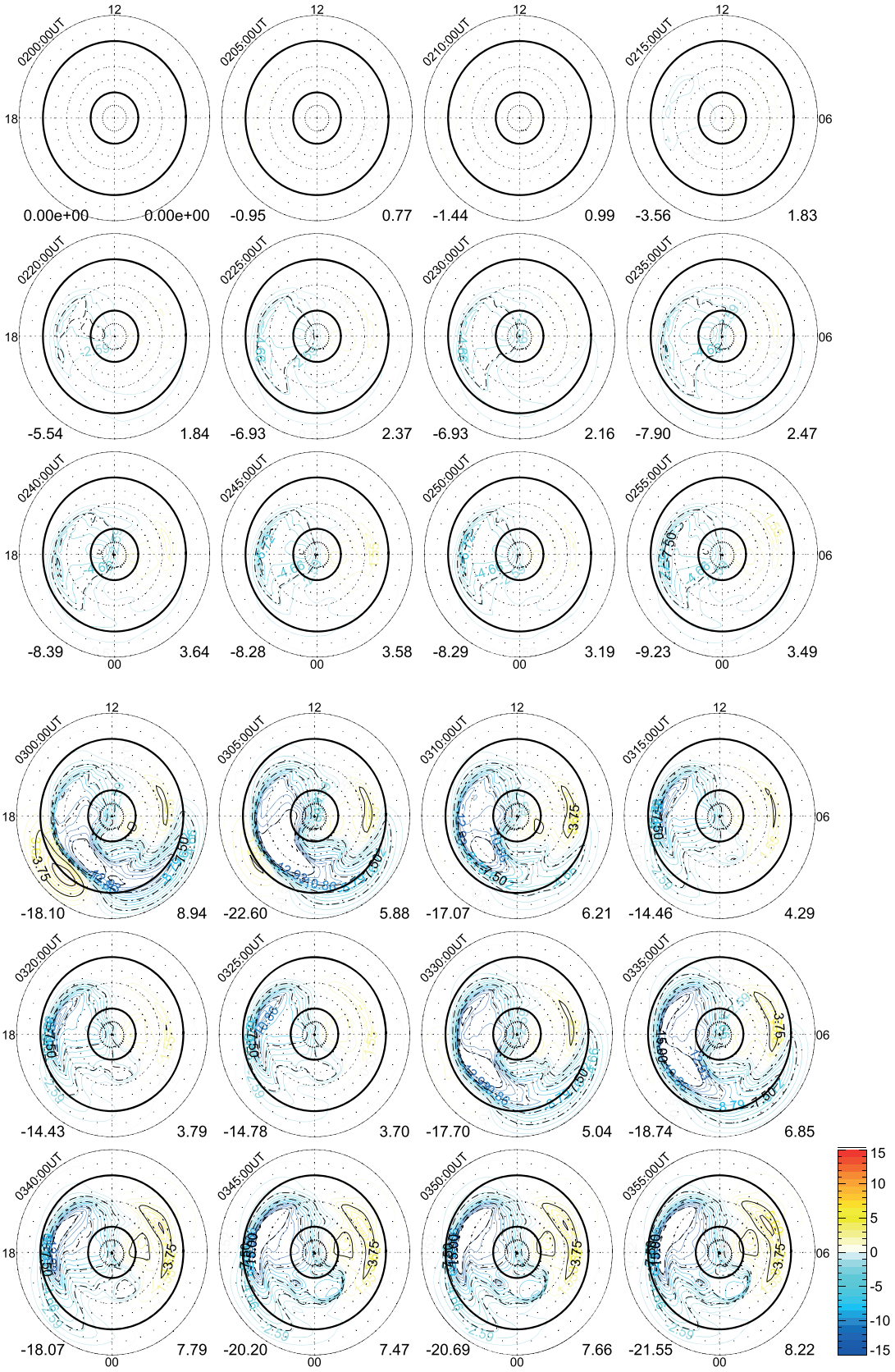

Figure 6. Residual ionospheric electric potential patterns after 02:00. The base potential pattern that is used to be subtracted is at 02:00. The circle plots are in 5 min cadence. Blue contour lines indicate a decrease in the potential compared with that at 02:00 and yellow contour lines indicate an increase in the potential. The unit of potential is kV.

ascribed to the KH surface waves that allow more solar wind energy into the magnetosphere.

[21] Careful inspection of the increase in the CPCP index after 02:00 reveals that the local peaks in the index are highly correlated to the KHI occurrence. As mentioned in section 3, the largest penetration of magnetosheath plasma into the magnetosphere takes place four times at 02:20, 02:45, 03:15, and 03:50, respectively. Accordingly, the CPCP index reaches a local maximum approximately around these times (see the vertical lines). Figure 6 shows the ionospheric electric potential patterns from 02:00 to 04:00 after the 02:00 universal time potential is subtracted from them. The subtraction is done in order to observe the evolution in the ionosphere that would be difficult to see under southward IMF conditions in which the strong background of the ionospheric potential veils the subtle changes. Around 02:15, two convection vortices with the same polarity as the two-cell background pattern emerge and propagate toward the nightside while growing in magnitude. Such an emerge-grow-and-propagate behavior is also observed starting from time 03:15 and 03:50, which is consistent with the time that KH vortex appears on the flanks and then propagates tailward. Such a connection of KH waves on the magnetopause boundary and the ionospheric electrodynamics implies that even with constant solar wind driving, the geospace system can gain additional energy via the surface waves. The above connection ultimately completes the solar wind-magnetosphere-ionosphere coupling circulation: the ionospheric mass outflow into the magnetosphere varies the magnetospheric dynamics as well as solar wind-magnetosphere interaction by triggering the KH surface waves, which transfers additional solar wind energy into the magnetosphere, influencing the ionospheric electrodynamics. This can theoretically further change the initial characteristics of the ionospheric mass outflow, the first driver in this circulation. However, the correlation between the energy deposited and the subsequent ionospheric outflow is not included in this study since the imposed outflow is forced to be constant throughout the simulation. Future studies will focus on a more self-consistent outflow by including a causal relationship between the energy input and the ionospheric outflow, such as the empirical relationship derived by *Strangeway et al.* [2005].

5. Conclusion

[22] To explore the dependence of the magnetosphere on the characteristics of the ionospheric outflow, this study investigated the effect of ionospheric outflow intensity. Two different uniform outflow intensities are specified in the polar region of an MHD model: one with a fluence rate of 9×10^{25} ions/s and another with a fluence of 2×10^{26} ions/s. Although these two numerical experiments use idealized constant outflow densities simply applied over the polar cap region, the total fluence rate is consistent with observations. Results indicate that a larger ionospheric outflow intensity plays a more profound role in altering the global magnetosphere configuration.

[23] The O^+ outflow with a larger intensity greatly disturbs the global magnetosphere by triggering Kelvin-Helmholtz surface waves along the magnetopause boundary with an off-equator propagation angle of about 20°. These waves increase the solar wind-magnetosphere coupling efficiency by increasing the reconnection rate through the roll up of Kelvin-Helmholtz vortices. The CPCP index subsequently increases after its initial reduction. This simulation also suggests that the Kelvin-Helmholtz instability (KHI), preferentially occurring during northward IMF conditions, can be triggered even with southward IMF given certain conditions, such as when a large supply of heavy ions of ionospheric origin is present in the magnetosphere. This implies that the ionospheric heavy ions can be another crucial factor, besides the commonly recognized factor—the elevated solar wind speed, in exciting the instability on the magnetopause boundary. The increased ionospheric mass source that usually occurs during storm time causes an increased probability of KHI, which may allow more solar wind plasma into the magnetosphere. This suggests that there is a possibility of even further nonlinear coupling between the magnetosphere and solar wind.

[24] **Acknowledgments.** The work at UM was supported by NSF ATM0639336, ANT0838828, and DoD FA95550-07-1-0434, and the work at LANL was supported by the U.S. Department of Energy through the Los Alamos National Laboratory/Laboratory Directed Research and Development (LDRD) program.

[25] Masaki Fujimoto thanks the reviewer for assistance in evaluating this paper.

References

Borovsky, J. E., M. Hesse, J. Birn, and M. M. Kuznetsova (2008), What determines the reconnection rate at the dayside magnetosphere?, *J. Geophys. Res.*, *113*, A07210, doi:10.1029/2007JA012645.

Bouhram, M., et al. (2005), Survey of energetic O^+ ions near the dayside mid-latitude magnetopause with Cluster, *Ann. Geophys.*, *23*, 1281–1294.

Brambles, O. J., W. Lotko, P. A. Damiano, B. Zhang, M. Wiltberger, and J. Lyon (2010), Effects of causally driven cusp O^+ outflow on the storm time magnetosphere-ionosphere system using a multifluid global simulation, *J. Geophys. Res.*, *115*, A00J04, doi:10.1029/2010JA015469.

Brambles, O. J., W. Lotko, B. Zhang, M. Wiltberger, J. Lyon, and R. J. Strangeway (2011), Magnetosphere sawtooth oscillations induced by ionospheric outflow, *Science*, *332*, 1183–1186, doi:10.1126/science.1202869.

Claudepierre, S. G., S. R. Elkington, and M. Wiltberger (2008), Solar wind driving of magnetospheric ULF waves: Pulsations driven by velocity shear at the magnetopause, *J. Geophys. Res.*, *113*, A05218, doi:10.1029/2007JA012890.

Cully, C. M., E. F. Donovan, A. W. Yau, and G. G. Arkos (2003), Akebono/Suprathermal Mass Spectrometer observations of low-energy ion outflow: Dependence on magnetic activity and solar wind conditions, *J. Geophys. Res.*, *108*(A2), 1093, doi:10.1029/2001JA009200.

Daglis, I. A., and W. I. Axford (1996), Fast ionospheric response to enhanced activity in geospace: Ion feeding of the inner magnetotail, *J. Geophys. Res.*, *101*, 5047–5066, doi:10.1029/95JA02592.

De Zeeuw, D. L., S. Sazykin, R. A. Wolf, T. I. Gombosi, A. J. Ridley, and G. Tóth (2004), Coupling of a global MHD code and an inner magnetospheric model: Initial results, *J. Geophys. Res.*, *109*, A12219, doi:10.1029/2003JA010366.

Garcia, K. S., V. G. Merkin, and W. J. Hughes (2010), Effects of nightside O^+ outflow on magnetospheric dynamics: Results of multifluid MHD modeling, *J. Geophys. Res.*, *115*, A00J09, doi:10.1029/2010JA015730.

Glocer, A., G. Tóth, T. Gombosi, and D. Welling (2009a), Modeling ionospheric outflows and their impact on the magnetosphere, initial results, *J. Geophys. Res.*, *114*, A05216, doi:10.1029/2009JA014053.

Glocer, A., G. Tóth, Y. Ma, T. Gombosi, J. Zhang, and L. M. Kistler (2009b), Multifluid Block-Adaptive-Tree Solar wind Roe-type Upwind Scheme: Magnetospheric composition and dynamics during geomagnetic storms—initial results, *J. Geophys. Res.*, *114*(12), A12203, doi:10.1029/2009JA014418.

Gratton, F. T., L. Bender, C. J. Farrugia, and G. Gnavi (2004), Concerning a problem on the Kelvin-Helmholtz stability of the thin magnetopause, *J. Geophys. Res.*, *109*, A04211, doi:10.1029/2003JA010146.

Hasegawa, A. (1975), Plasma instabilities and nonlinear effects, *Springer Verlag Springer Series on Physics Chemistry Space*, *8.*

Hasegawa, H., M. Fujimoto, T. Phan, H. Rème, A. Balogh, M. W. Dunlop, C. Hashimoto, and R. TanDokoro (2004), Transport of solar wind into Earth's magnetosphere through rolled-up Kelvin–Helmholtz vortices, *Nature*, *430*, 755–758, doi:10.1038/nature02799.

Hwang, K.-J., M. M. Kuznetsova, F. Sahraoui, M. L. Goldstein, E. Lee, and G. K. Parks (2011), Kelvin-Helmholtz waves under southward interplanetary magnetic field, *J. Geophys. Res.*, *116*, A08210, doi:10.1029/2011JA016596.

Kistler, L. M., C. G. Mouikis, B. Klecker, and I. Dandouras (2010), Cusp as a source for oxygen in the plasma sheet during geomagnetic storms, *J. Geophys. Res.*, *115*, A03209, doi:10.1029/2009JA014838.

Kistler, L. M. et al. (2005), Contribution of nonadiabatic ions to the cross-tail current in an O^+ dominated thin current sheet, *J. Geophys. Res.*, *110*, A06213, doi:10.1029/2004JA010653.

Kivelson, M., and S.-H. Chen (1995), *The Magnetopause: Surface Waves and Instabilities and Their Possible Dynamical Consequences*, 257 p., AGU, Washington, D. C.

Li, L. Y., J. B. Cao, G. C. Zhou, T. L. Zhang, D. Zhang, I. Dandouras, H. Reme, and C. M. Carr (2011), Multiple responses of magnetotail to the enhancement and fluctuation of solar wind dynamic pressure and the southward turning of interplanetary magnetic field, *J. Geophys. Res.*, *116*, A12223, doi:10.1029/2011JA016816.

Liao, J., L. M. Kistler, C. G. Mouikis, B. Klecker, I. Dandouras, and J.-C. Zhang (2010), Statistical study of O^+ transport from the cusp to the lobes with Cluster CODIF data, *J. Geophys. Res.*, *115*, A00J15, doi:10.1029/2010JA015613.

Liao, J., L. M. Kistler, C. G. Mouikis, B. Klecker, and I. Dandouras (2012), Solar cycle dependence of the cusp O^+ access to the near-Earth magnetotail, *J. Geophys. Res.*, *117*, A10220, doi:10.1029/2012JA017819.

Liu, Y., L. M. Kistler, C. G. Mouikis, B. Klecker, and I. Dandouras (2013), Heavy ion effects on substorm loading and unloading in the Earth's magnetotail, *J. Geophys. Res. Space Physics*, *118*, 2101–2112, doi:10.1002/jgra.50240.

Lyon, J. G., J. A. Fedder, and C. M. Mobarry (2004), The Lyon-Fedder-Mobarry (LFM) global MHD magnetospheric simulation code, *J. Atmos. Sol. Terr. Phys.*, *66*, 1333–1350, doi:10.1016/j.jastp.2004.03.020.

Moore, T. E., M.-C. Fok, S. P. Christon, S.-H. Chen, M. O. Chandler, D. C. Delcourt, J. Fedder, S. Slinker, and M. Liemohn (2005), Solar and ionospheric plasmas in the ring current region, in *Inner Magnetosphere Interactions: New Perspectives From Imaging, Geophys. Monogr. Ser.,* vol. 159, edited by J. Burch, M. Schulz, and H. Spence, pp. 179–194, AGU, Washington, D. C.

Nakamura, T. K. M., M. Fujimoto, and A. Otto (2008), Structure of an MHD-scale Kelvin-Helmholtz vortex: Two-dimensional two-fluid simulations including finite electron inertial effects, *J. Geophys. Res.*, *113*, A09204, doi:10.1029/2007JA012803.

Nosé, M., S. Taguchi, K. Hosokawa, S. P. Christon, R. W. McEntire, T. E. Moore, and M. R. Collier (2005), Overwhelming O^+ contribution to the plasma sheet energy density during the October 2003 superstorm: Geotail/EPIC and IMAGE/LENA observations, *J. Geophys. Res.*, *110*, A09S24, doi:10.1029/2004JA010930.

Nykyri, K., and A. Otto (2001), Plasma transport at the magnetospheric boundary due to reconnection in Kelvin-Helmholtz vortices, *Geophys. Res. Lett.*, *28*, 3565–3568, doi:10.1029/2001GL013239.

Pegoraro, F., M. Faganello, and F. Califano (2008), Collisionless Kelvin-Helmholtz instability and vortex-induced reconnection in the external region of the Earth magnetotail, *J. Phys. Conf. Ser*, *133*(1), 012024, doi:10.1088/1742-6596/133/1/012024.

Powell, K. G., P. L. Roe, T. J. Linde, T. I. Gombosi, and D. L. D. Zeeuw (1999), A solution-adaptive upwind scheme for ideal magnetohydrodynamics, *J. Comp. Phys.*, *154*, 284.

Ridley, A. J., T. I. Gombosi, and D. L. D. Zeeuw (2004), Ionospheric control of the magnetospheric configuration: Conductance, *Ann. Geophys.*, *22*, 567–584.

Ridley, A. J. (2006), The magnetospheric and ionospheric response to a very strong interplanetary shock and coronal mass ejection, *Adv. Space Res.*, *38*, 263–272, doi:10.1016/j.asr.2006.06.010.

Russell, C. T., and R. C. Elphic (1979), ISEE observations of flux transfer events at the dayside magnetopause, *Geophys. Res. Lett.*, *6*, 33–36, doi:10.1029/GL006i001p00033.

Strangeway, R. J., R. E. Ergun, Y. Su, C. W. Carlson, and R. C. Elphic (2005), Factors controlling ionospheric outflows as observed at intermediate altitudes, *J. Geophys. Res.*, *110*, A03221, doi:10.1029/2004JA010829.

Toffoletto, F., S. Sazykin, R. Spiro, and R. Wolf (2003), Inner magnetospheric modeling with the Rice Convection Model, *Space Sci. Rev.*, *107*, 175–196, doi:10.1023/A:1025532008047.

Welling, D. T., and A. J. Ridley (2010), Validation of SWMF magnetic field and plasma, *Space Weather*, *8*, S03002, doi:10.1029/2009SW000494.

Welling, D. T., and S. G. Zaharia (2012), Ionospheric outflow and cross polar cap potential: What is the role of magnetospheric inflation? *Geophys. Res. Lett.*, *39*, L23101, doi:10.1029/2012GL054228.

Wiltberger, M., W. Lotko, J. G. Lyon, P. Damiano, and V. Merkin (2010), Influence of cusp O^+ outflow on magnetotail dynamics in a multifluid MHD model of the magnetosphere, *J. Geophys. Res.*, *115*, A00J05, doi:10.1029/2010JA015579.

Winglee, R. M. (2003), Circulation of ionospheric and solar wind particle populations during extended southward interplanetary magnetic field, *J. Geophys. Res.*, *108*(A10), 1385, doi:10.1029/2002JA009819.

Winglee, R. M., D. Chua, M. Brittnacher, G. K. Parks, and G. Lu (2002), Global impact of ionospheric outflows on the dynamics of the magnetosphere and cross-polar cap potential, *J. Geophys. Res.*, *107*(A9), 1237, doi:10.1029/2001JA000214.

Wolf, R. A. (1983), The quasi-static (slow-flow) region of the magnetosphere, in *Solar Terrestrial Physics*, edited by R. L. Carovillano and J. M. Forbes, pp. 303–368, D. Reidel Publishing, Hingham, MA.

Yu, Y., and A. J. Ridley (2008), Validation of the space weather modeling framework using ground-based magnetometers, *Space Weather*, *6*, S05002, doi:10.1029/2007SW000345.

Yu, Y., and A. J. Ridley (2011), Understanding the response of the ionosphere-magnetosphere system to sudden solar wind density increases, *J. Geophys. Res.*, *116*, A04210, doi:10.1029/2010JA015871.

Yu, Y., and A. J. Ridley (2013), Exploring the influence of ionospheric O^+ outflow on magnetospheric dynamics: Dependence on the source location, *J. Geophys. Res. Space Physics*, *118*, 1711–1722, doi:10.1029/2012JA018411.

Yu, Y., A. J. Ridley, D. T. Welling, and G. Tóth (2010), Including gap region field-aligned currents and magnetospheric currents in the MHD calculation of ground-based magnetic field perturbations, *J. Geophys. Res.*, *115*, A08207, doi:10.1029/2009JA014869.